Biomaterials 35 (2014) 9114–9125

Contents lists available at ScienceDirect

Biomaterials

journal homepage: www.elsevier.com/locate/biomaterials

In vitro and *in vivo* anti-biofilm effects of silver nanoparticles immobilized on titanium

Hui Qin [a, 1], Huiliang Cao [b, 1], Yaochao Zhao [a], Cheng Zhu [a], Tao Cheng [a], Qiaojie Wang [a], Xiaochun Peng [a], Mengqi Cheng [a], Jiaxin Wang [a], Guodong Jin [b], Yao Jiang [a], Xianlong Zhang [a, **], Xuanyong Liu [b, *], Paul K. Chu [c]

[a] Department of Orthopedics, Shanghai Sixth People's Hospital, Shanghai Jiao Tong University, Shanghai 200233, China
[b] State Key Laboratory of High Performance Ceramics and Superfine Microstructure, Shanghai Institute of Ceramics, Chinese Academy of Sciences, Shanghai 200050, China
[c] Department of Physics & Materials Science, City University of Hong Kong, Tat Chee Avenue, Kowloon, Hong Kong, China

ARTICLE INFO

Article history:
Received 15 May 2014
Accepted 23 July 2014
Available online 8 August 2014

Keywords:
Silver nanoparticles
Titanium
Biofilm
Cytotoxicity
Plasma immersion ion implantation

ABSTRACT

Prevention of periprosthetic infection (PPI) by inhibiting biofilm formation on prostheses is crucial to orthopedic surgery. In this work, silver nanoparticles (Ag NPs) are fabricated *in situ* and immobilized on titanium by silver plasma immersion ion implantation (PIII). The anti-biofilm activity rendered by the immobilized Ag NPs is assessed using *Staphylococcus epidermidis*, a biofilm producing strain, *in vitro* and *in vivo*. The immobilized Ag NPs show no apparent cytotoxicity but reduce biofilm formation *in vitro* by inhibiting bacteria adhesion and *icaAD* transcription. The immobilized Ag NPs offer a good defense against multiple cycles of bacteria attack *in vitro*, and the mechanism is independent of silver release. Radiographic assessment, microbiological cultures, and histopathological results demonstrate the ability of the functionalized surface against bacterial infection to reduce the risk of implant-associated PPI.

1. Introduction

Serum protein accumulation on biomedical implants is one of the causes of bacteria adhesion [1]. The adherent bacteria synthesize a complex glycocalyx to form a biofilm that protects microorganisms from antibiotic treatment [2,3] leading to periprosthetic infection (PPI) [4]. PPI happens in 1%–2% of primary arthroplasties [5,6] and the occurrence rate can be greater than 10% in secondary arthroplasties [5–8]. If PPI occurs, patients may need to undergo multiple surgeries together with antibiotic therapy for an extended period of time resulting in suffering and even disability [4]. In some cases, PPI persists in spite of treatment [9] and so prevention of PPI is very important. As biofilm formation is the key to PPI, new strategies that prevent biofilm formation are demanded by the orthopedic community.

Several methods have been proposed to counteract PPI [1,10–15], for instance, controlled local release systems such as bone cement impregnated with antibiotics, but there are a number of shortcomings such as local tissue damage due to explosive release in the early stage [1], activity degradation as the agent is consumed, and resistance to antibiotics [16,17]. Silver nanoparticles (Ag NPs) have promising antibacterial activity and can be integrated into a controlled-release platform [18] due to the small size and high mobility, but potential cytotoxicity at a high dosage is a concern. Furthermore, mobile Ag NPs may enter mammalian cells and adversely alter intracellular functions [19,20]. Hence, restricting the mobility of Ag NPs by immobilization is crucial to clinical success [21–23]. In our previous work, Ag NPs were produced on titanium by silver plasma immersion ion implantation (Ag-PIII) and the immobilized Ag NPs exhibited good antibacterial activity and cytocompatibility *in vitro* [21]. However, the possible anti-biofilm mechanism and *in vivo* characteristics of the Ag NPs immobilized by this technique are not well understood. In this work, the biofilm inhibition capability is investigated systematically using *Staphylococcus epidermidis* (*S. epidermidis*, ATCC 35984), a biofilm producing strain [24]. The composition, bacteria amount, structure, and related gene expression of the biofilm as well as longevities of the anti-biofilm activity are assessed *in vitro* and a model involving implant-related tibia osteomyelitis in rats, which can simulate PPI [25,26] is adopted to evaluate the effectiveness *in vivo*.

* Corresponding author. Tel./fax: +86 21 5241 2409.
** Corresponding author. Tel.: +86 21 6436 9183; fax: +86 21 6470 1363.
E-mail addresses: zhangxianl197826@163.com (X. Zhang), xyliu@mail.sic.ac.cn (X. Liu).
[1] These authors contributed equally to this work.

http://dx.doi.org/10.1016/j.biomaterials.2014.07.040
0142-9612/

2. Materials and methods

2.1. Sample preparation and characterization

In the *in vitro* experiments, the samples were acid-etched 10 mm and 20 mm square commercial pure titanium (Cp Ti, Grade 2) plates with a thickness of 1 mm and the samples used in the *in vivo* assessment were 40 mm long and 0.8 mm diameter Cp Ti Kirschner wires. Ag NPs were fabricated and immobilized *in situ* on the Ti samples by a cathodic arc silver plasma immersion ion implantation (Ag-PIII) process [21]. The important PIII instrumental parameters are listed in Table 1. After ultrasonic cleaning, the Ag-PIII samples were sterilized in an autoclave at 121 °C for 40 min prior to further use.

Four groups of samples were tested, namely commercial pure titanium (control, denoted as Cp Ti) and three Ag-PIII Ti samples implanted for 0.5 h, 1.0 h, and 1.5 h (designated as 0.5 h-Ag-PIII, 1.0 h-Ag-PIII, and 1.5 h-Ag-PIII, respectively). The surface morphology was examined by field-emission scanning electron microscopy (FE-SEM, JEOL JSM-6700F, Tokyo, Japan) and the surface composition and chemical states were determined by x-ray photoelectron spectroscopy (XPS, PHI 5802, Physical Electronics Inc., Eden Prairie, MN).

The Ag-PIII titanium plates were soaked in 10 ml of phosphate-buffered saline solution (PBS) at 37 °C for two months without stirring. The amounts of released silver were determined by analyzing the solutions by inductively-coupled plasma optical emission spectrometry (ICP-OES, Nu Instruments, Wrexham, UK).

2.2. In vitro cytotoxicity evaluation

In order to compare the cytotoxicity between the mobile and immobilized Ag NPs, Ag NPs particles (average diameter of 20 nm, Huzheng Nano Technology Limited Company, Shanghai, China) with a concentration of 2 mg/ml were used in the parallel study. MC3T3-E1 cells were employed to assess the cytotoxicity. The 10 mm square samples were placed on 24 well plates on which the cells were seeded at a density of 2×10^4/well. After 24 h, the samples were transferred to new 24 well plates and then 1 ml of the growth medium consisting of α-minimum essential medium (α-MEM) (Gibco, Invitrogen, Inc) supplemented with 10% fetal bovine serum (FBS, Gibco) containing different concentrations of the mobile Ag NPs were added to the wells containing the Cp Ti samples. The other wells contained Cp Ti or Ag-PIII samples and were cultured with the growth medium without the mobile Ag NPs for 1 and 3 days. The cytotoxicity was assessed using the Cell Counting Kit-8 assay (CCK-8, Beyotime). After each incubation period, the culture medium was removed and 1.0 ml of the fresh medium with 10% CCK-8 was added to each well. After incubation for 4 h, 100 μl of the culture medium was transferred to a 96 well plate for measurement. The absorbance was measured on an enzyme labeling instrument (BIO-TEK, ELX 800) at a wavelength of 450 nm. For comparison with the embedded Ag NPs, the volume of a single mobile silver nanoparticle is calculated using the following formula: $v = 4/3\pi r^3$ and the amount of Ag NPs: $n = m/\rho v$ (r represents the radius, m is the mass, and ρ is the density of Ag being 10.53 g/cm^3) [27].

2.3. Bacteria preparation and characterization

Freeze-dried *S. epidermidis* (ATCC 35984) was obtained from the American Type Culture Collection (Rockefeller, MD) and the species identification test was completed on the Vitek 2 automated system (BioMèrieux, Marcy l'Etoile, France). The biofilm formation ability was assessed on a microtiter plate (MtP) [28,29]. The strains with optical density (OD) values less than 0.120 were considered as negative; those with OD values between 0.120 and 0.240 were regarded as weak biofilm producers, and strains with OD values greater than 0.240 were indicative of biofilm producing bacterial strains. The ability of producing biofilms was confirmed by the *ica*A expression.

2.4. Determination of biofilm formation

The surface biofilms were analyzed by crystal violet staining, spread plate method, CLSM, and SEM. The inocula of the strain were prepared by adjusting the concentration of an overnight bacterial broth cultured to 1×10^6 colony forming units (CFUs)/ml in Trypticase Soy Broth (TSB; BD Biosciences, Franklin Lakes, NJ) supplemented with 0.25% (w/v) glucose (TSBG) as determined by McFarland. 100 μl of the bacteria suspension was added to the surface of the four samples on a 24 well plate and statically incubated at 37 °C for 6, 12 and 24 h. At each time point, the samples were gently washed with PBS three times to remove loosely adherent bacteria.

Table 1
Important Ag-PIII parameters.

	Target	Cathodic arc
Voltage pulse duration (μs)	500	500
Pulsing frequency (Hz)	5	5
Bias voltage (kV)	−30	/
Pressure (Pa)	5×10^{-3}	/

2.4.1. Bacterial biofilm formation assay by crystal violet staining

The samples were stained with 1 ml of PBS containing 100 μl of 1% (*w*/*v*) crystal violet, incubated at room temperature for 15 min, and washed with PBS three times. After adding 1 ml of 95%(*v*/*v*) EtOH to each well, the plate was shaken for 15 min to release the dye from the biofilms and the absorbance was determined on an enzyme labeling instrument (BIO-TEK, ELX 800) at 570 nm [30].

2.4.2. Bacterial biofilm formation assay by the spread plate method

The samples were placed in 1 ml of PBS, and the adherent bacteria attached to the surface were collected ultrasonically for 5 min in a 150 W ultrasonic bath (B3500S-MT, Branson Ultrasonics Co., Shanghai, China) at a frequency of 50 Hz after rapid vortex mixing (Vortex Genie 2, Scientific Industries, Bohemia, NY, USA) at the maximum power for 1 min [24]. The solutions were serially diluted 10 folds, plated in triplicate onto sheep blood agar (SBA), and incubated at 37 °C for 24 h. The number of CFUs on the SBA was counted in accordance with the National Standard of China GB/T 4789.2 protocol. The antibacterial rates (Ra) for adhered bacteria on the samples were calculated based on the following formulas: (Ra) (%) = $(A - B)/A \times 100\%$ where A indicated the average number of viable bacteria on the Cp Ti and B was the average number of viable bacteria on the Ag-PIII specimens.

2.4.3. Bacterial biofilm formation assay by CLSM

The samples were placed on a new 24 well plate, stained with 500 μl of combination dye (LIVE/DEAD BacLight bacteria viability kits, Invitrogen) for 15 min, and examined by confocal laser scanning microscopy (LSM 510 meta; Zeiss, Germany). The viable bacteria with intact cell membrane were stained green whereas nonviable bacteria with damaged membranes were stained red.

2.4.4. Bacterial biofilm formation assay by SEM

The samples were fixed with 2.5% glutaraldehyde for 4 h, dehydrated in the graded ethanol series (30, 50, 70, 80, 90, and 100 *v*/*v*%) for 10 min each sequentially, dehydrated in absolute ethanol (twice), freeze dried, coated with gold, and examined by scanning electron microscopy (JEOL JSM-6310LV, Japan).

2.4.5. qRT-PCR analysis of icaAD and icaR transcription

The biofilm associated genes were quantitatively analyzed by real-time PCR. 500 μl of the bacteria suspension were added to the surface of 20 mm square samples on a 6 well plate and statically incubated at 37 °C for 24 h. The biofilm bacteria were harvested by sonicating and vortexing. The bacteria were pelleted by centrifugation at 10,000 g for 5 min and then resuspended in 200 μl of TE buffer (10 mM Trise HCl, 1 mM EDTA, pH 7.0) containing 100 mg/ml of lysostaphin (Sigma) and incubated at 37 °C for 10 min [24]. The total RNA was extracted by TRIzol (Invitrogen). One microgram of the total RNA was reverse transcribed into complementary DNA (cDNA) using the PrimeScript RT reagent Kit (Takara). The qRT-PCR analysis was performed on the Bio-Rad C1000 using SYBR Premix Ex Taq II (Takara) and the primers for the target genes are listed in Table 2. The expression levels of *icaAD* and *icaR* were evaluated and normalized to the internal standard gene 16S rRNA.

2.5. Longevity and stability of the antibacterial activity

To assess the long-term antibacterial activity, the samples were incubated in PBS for up to 60 days. At selected time points (1, 7, 14, 20, 40, 60d), the samples were supplied with 1×10^6 cfu/ml bacteria suspension for 24 h. To evaluate the stability of the antibacterial activity, the samples were incubated with the above bacteria suspension for 24 h, ultrasonically cleaned, sterilized, and re-inoculated as aforementioned. This process was repeated every two days for seven times and the Ra value of the adhered bacteria on the specimens of the two tests was calculated.

2.6. Effects of serum on antibacterial activity

The samples were incubated with complete FBS or PBS statically at 37 °C on a 24 well plate for 48 h and transferred to a fresh plate. 100 μl of the 1×10^6 cfu/ml bacteria suspension were added to the surface of the samples for 24 h prior to the spread plate evaluation.

Table 2
Primers used in this study.

Target gene	Direction	Primer sequence (5′–3′)
icaA	F	AACAAGTTGAAGGCATCTCC
	R	GATGCTTGTTTGATTCCCT
icaD	F	ATCGTTGTGATGATTGTTTA
	R	GATATGTCACGACCTTTCTT
icaR	F	CCATTGACGGACTTTACCAG
	R	CAAAGCGATGTGCGTAGGA
16S rRNA	F	TCGTGTCGTGAGATGTTGGGTTA
	R	GGTTTCGCTGCCCTTTGTATTGT

F-forward; R-reverse.

2.7. Implant-related tibia osteomyelitis model in rats

The experimental protocol was approved by the Animal Care and Experiment Committee of Sixth Peoples Hospital affiliated to Shanghai Jiao Tong University, School of Medicine. Sixty male Sprague Dawley rats 4 months in age and weighing an average of 255 g (180–300 g) were used. The surgery was performed under general anesthesia by weight-adopted intraperitoneal injection of 4% chloral hydrate (0.9 ml/100 g body wt). The animals were prepared as follows. The left hind leg was shaved and disinfected with povidone iodine. To provide sterile conditions during surgery, the animals were placed on sterile gauzes soaked with povidone iodine and the bodies were covered with sterile sheets. 0.5 cm longitudinal incision was made to the anteromedial aspect of the tibia. To access the medullary cavity, a hole between the tibial plateau and tibial tuberosity was drilled by hand with a steel Kirschner wire (1.0 mm in diameter) through the cancellous bone of the proximal metaphysic. The surrounding periosteum remained intact. The steel Kirschner wire was inserted into the medullary cavity and pushed forward distally for smooth dilatation of the cavity. After removal, 10 μl of either PBS or PBS containing ATCC 35984 at a concentration of 1×10^5 cfu/ml was injected into the medullary cavity by a 50 μl microsyringe. According to the study groups, six groups (Table 3) were investigated.

After bacterial inoculation, an Ag-PIII or Ti Kirschner wire (diameter: 0.8 mm) was inserted. The protruding portion of the Kirschner wire was cut off at the site of entry. The soft tissue was irrigated with povidone iodine solution, and the skin and fascia were sutured. Following surgery, the animals were housed in separate cages and allowed to eat and drink adlibitum. Weight bearing was started immediately postoperatively, and the animals were monitored daily. Buprenorphine was administered for 2 days as an analgesic but no antibiotic was administered.

2.8. Animal weight, temperature and blood analyses

At 0, 3, 7, 14, 21, 28, 35, and 42 days post-surgery, the rectal body temperature was measured by a digital thermometer, and the body weight was determined on a precision scale. 0.5 ml of blood was taken from the ophthalmic vein plexus and analyzed for hemoglobin and white blood cell count.

2.9. Radiographic evaluation

At 0, 2, 4, 6 weeks post-surgery, high-resolution lateral radiographs were obtained when the animals were under general anesthesia with chloral hydrate. Three independent observers with no prior knowledge of the study group evaluated the radiographs focusing on three regions of interest (ROI): (1) proximal epi-/metaphyseal area, (2) diaphyseal region, and (3) distal epi-/metaphyseal area. The radiographic evaluation was based on a system used by Lucke et al. [25]. The following radiographic appearances were evaluated for each ROI: (1) Periosteal reaction, (2) Soft tissue swelling, (3) Osteolysis, (4) General impression, and (5) Deformity. The appearances were given a score as follows: 0 = absent, 1 = mild, 2 = moderate, or 3 = severe. In addition, (6) sequestra formation and (7) spontaneous fracture were evaluated for each tibia as a whole and given a score of 0 = absent or 1 = present. The maximum score was 47.

2.10. Microbiological evaluation

After 42 days, the animals were sacrificed and 3 ml of blood was collected from the right atrium for aerobic culture. Both tibiae were aseptically retrieved. All soft tissues were removed, and bones were weighed on a precision scale after the Kirschner wires were explanted. The weight difference between the experimental side and contralateral tibia was recorded. The explanted Kirschner wires were rolled over SBA for semi-quantification of bacteria adhesion on the Kirschner wires. To quantify bacteria adhesion, they were placed in 4 ml PBS, sonicated, and vortexed to dislodge adhered bacteria. Using the spread plate method discussed above, the adhered bacteria were counted. The bacteria isolated from blood cultures and agar plates were identified using the above methods.

Five tibiae of every group were randomly chosen, snap frozen, and ground to powder under sterile conditions [31]. Then bone powder of one tibia was agitated in 2 ml of PBS for 3 min. After centrifuging at 10,000 g for 15 s, the supernatant was withdrawn for serial (10-fold) dilution, and the samples were analyzed for CFU/tibia by the spread plate method.

Table 3
Details of animal experiments.

Group	Number (n)	Implant	Inoculation
I	10	Ti wire	*S. epidermidis* 10^3 CFU/10 μl
II	10	0.5 h-Ag-PIII Ti wire	*S. epidermidis* 10^3 CFU/10 μl
III	10	1.0 h-Ag-PIII Ti wire	*S. epidermidis* 10^3 CFU/10 μl
IV	10	1.5 h-Ag-PIII Ti wire	*S. epidermidis* 10^3 CFU/10 μl
V	10	Ti wire	PBS/10 μl
VI	10	No	*S. epidermidis* 10^3 CFU/10 μl

2.11. Histopathological evaluation

The remaining five tibiae of each group were fixed in 10% neutral buffered formalin for 48 h, dehydrated in alcohol solutions, and embedded in methyl methacrylate (Technovit9100, Heraeus, Wehrheim, Germany). Longitudinal sections in a sagittal plane were cut at 10 μm by a RM 2155 Microtome (Leica, Bensheim, Germany). Masson's Trichrome staining was implemented to examine the morphology and Giemsa staining was adopted to evaluate bacterial contamination. Three independent "blinded" observers evaluated the bone histology focusing on four ROI: (1) proximal epi-/metaphysis, (2) proximal diaphysis, (3) distal diaphysis, and (4) distal epi-/metaphysis. Slices were evaluated using the method mentioned by Lucke et al. [25]. The following histological changes were evaluated for each ROI: (1) Sequestrum formation, (2) Enlargement of corticalis, (3) Abscess formation, (4) Destruction of corticalis, and (5) General impression. Changes 1 to 4 were scored with 0 = absent or 1 = present and change 5 was scored with 0 = absent, 1 = mild, or 2 = severe. The maximum score was 24.

2.12. Statistical analysis

The experiments were conducted in triplicate and repeated three times and the data were expressed as means ± standard deviations. The one-way ANOVA and Student-Newman-Keuls post hoc tests were used to determine the level of significance and p values less than 0.05 and 0.01 were considered to be significant and highly significant, respectively.

3. Results

3.1. Material characterizations

The surface microstructure of the samples is shown in Fig. 1. Compared to the original surface of Cp Ti (Fig. 1a), homogeneously distributed spherical nanoparticles can be detected from the Ag-PIII samples (Fig. 1b–d). For 0.5 h-Ag-PIII, the particle diameter peak is about 18 nm (Fig. 1e) and there are about 1.52×10^7 particles per square millimeter. As the PIII duration is increased to 1.0 h, the particles become larger with a diameter peak at about 24 nm. The particle size distribution broadens but the particle density of $1.58 \times 10^7/mm^2$ is almost the same (Fig. 1f). However, as the Ag-PIII duration is increased to 1.5 h, the particle diameter distributions become bimodal with one peak at about 8 nm and the other at about 44 nm. The particle density increases to $1.81 \times 10^9/mm^2$ (Fig. 1g).

The samples are analyzed by XPS which reveals that the Cp Ti surface contains Ti and O but no Ag (Fig. 1h). As shown in Fig. 1i–k, the Ag 3d doublet at about 374.02 eV (Ag 3d3/2) and 368 eV (Ag 3d5/2) corresponding to metallic silver indicates that the Ag-PIII surface contains metallic silver [21,32]. These metallic silver nanoparticles (Ag NPs) are immobilized on the titanium surface as shown by TEM observation and XPS depth profiling [21]. Furthermore, the amounts of silver released from the Ag-PIII samples to PBS after two months are determined. The values obtained from 0.5 h-Ag-PIII, 1.0 h-Ag-PIII, and 1.5 h-Ag-PIII are 8.9, 10.5, and 10.9 ppb, respectively, indicating insignificant silver leaching from the Ag-PIII samples and effective immobilization.

3.2. In vitro cytotoxicity evaluation

A comparison of the cytotoxicity of the immobilized Ag NPs with mobile Ag NPs is carried out. As shown in Fig. 2, no obvious cytotoxicity relative to Cp Ti (control) is observed from the Ag-PIII samples. However, with regard to the mobile Ag NPs, significant cytotoxicity can be observed when the concentration reaches 8 μg/ml, although the amount of mobile Ag NPs in 1 ml of the solution at 8 μg/ml is almost the same as that on the 10 mm^2 1.5 h-Ag-PIII sample (~1.8×10^{11}), indicating that the cytotoxicity of immobilized Ag NPs is much less severe.

3.3. In vitro anti-biofilm property

Crystal violet staining assay is carried out to assess the biofilm inhibition activity. As shown in Fig. 3A, crystal violet absorption by

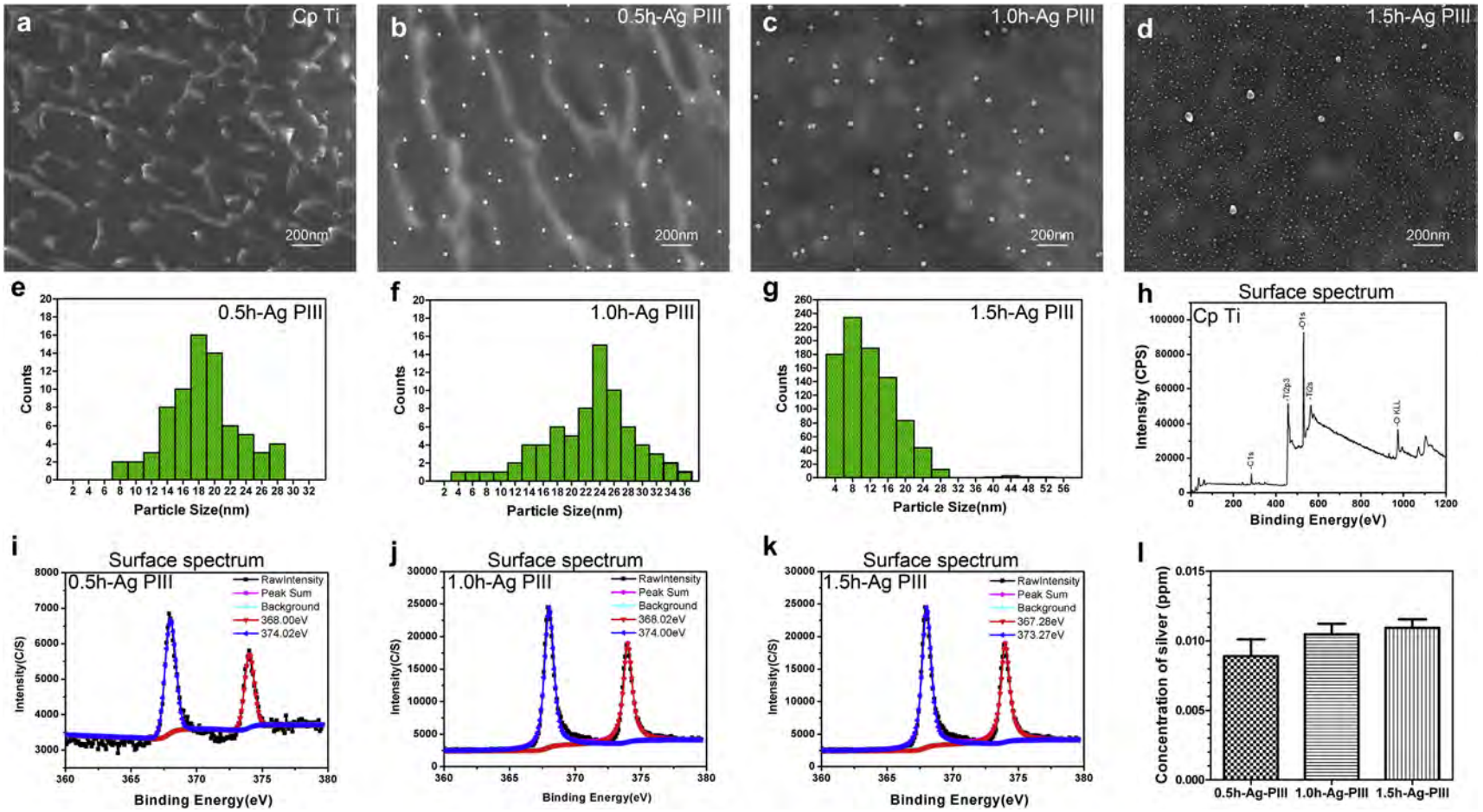

Fig. 1. Surface morphology of the titanium surface after Ag-PIII examined by SEM: (a) Cp Ti, (b) 0.5 h-Ag-PIII Ti, (c) 1.0 h-Ag-PIII Ti and (d) 1.5 h-Ag-PIII Ti; Size distributions of the particles on 0.5 h-Ag-PIII Ti (e), 1.0 h-Ag-PIII Ti (f) and 1.5 h-Ag-PIII Ti (g); XPS full spectra of Cp Ti (h) and XPS Ag 3d spectrum of Ag-PIII Ti surface: (i) 0.5 h-Ag-PIII Ti, (j) 1.0 h-Ag-PIII Ti and (k) 1.5 h-Ag-PIII Ti; (l) Silver release after Ag-PIII Ti soaking in PBS 60 days examined by ICP-MS.

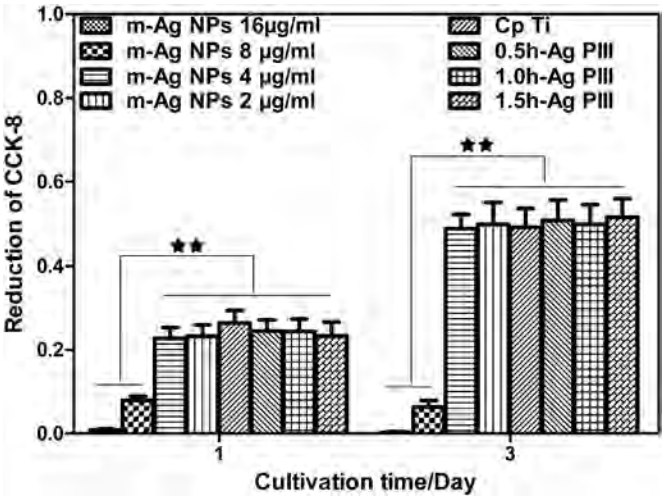

Fig. 2. Cytotoxic effects of the mobile Ag-NPs and embedded Ag-NPs on different concentrations of MC3T3-E1 cells. ★★, $p < 0.01$. m-Ag NPs meaning mobile Ag-NPs.

the Ag-PIII samples is substantially lower than that by Cp Ti at all the time points (6 h, 12 h, and 24 h). As the culturing duration is increased from 6 h to 24 h, crystal violet absorption by all the Ag-PIII samples increases slightly but that by Cp Ti shows a dramatic increase, demonstrating that Ag-PIII leads to good anti-biofilm effects. Among the Ag-PIII samples, 1.5 h-Ag-PIII shows the smallest increase suggesting that this sample is superior with regard to biofim inhibition.

The antibacterial rate (Ra) is quantitatively evaluated by the spread plate method. As shown in Fig. 3B, the Ra values of 0.5 h-Ag-PIII, 1.0 h-Ag-PIII, and 1.5 h-Ag-PIII increase from 64.9%, 78.8% and 83% at 6 h to 83.3%, 90.6% and 92.3% at 24 h, respectively, indicating that Ag-PIII can inhibit bacteria adhesion and proliferation. Compared to Cp Ti, 1.5 h-Ag-PIII has the strongest antibacterial activity.

The trend is confirmed by CLSM and SEM. The CLSM projected top-views of biofilm formation is shown in Fig. 4. As the culture duration is prolonged from 6 h to 24 h, the green fluorescent intensity (live bacterial colonies) on Cp Ti increases but decreases on the Ag-PIII samples, indicating that the Ag-PIII samples possess better antibacterial activity. A similar trend is observed by SEM. As shown in Fig. 5, from 6 h to 24 h, the amount of bacteria cells on Cp Ti increases and they conglomerate into grape-like colonie, indicating initiation of glycocalyx formation and characteristics of a biofilm [30]. In contrast, there are only a few bacteria cells on the Ag-PIII samples, suggesting that biofilm formation is indeed inhibited. Among the Ag-PIII samples, 1.5 h-Ag-PIII shows the least amount of bacteria cells, and the results are consistent with the results acquired by crystal violet staining, spread plate method, and CLSM.

Gene expression analysis (Fig. 6) indicates that the Ag-PIII samples inhibit biofilm formation by down-regulating the expression level of *icaA* and *icaD* but up-regulating the expression levels of *icaR*.

3.4. Longevity and stability of the anti-biofilm property

The anti-biofilm property of the Ag-PIII samples is determined after incubation in PBS for up to 60 days. As shown in Fig. 7A, the antibacterial rates, Ra, of 0.5 h-Ag-PIII, 1.0 h-Ag-PIII, and 1.5 h-Ag-PIII remain at 82.1%–85.9%, 85.4%–91.7%, and 92.6%–94.4%, indicating that the anti-biofilm activity of Ag-PIII is independent of silver release. The capability of the Ag-PIII in multiple bacteria attacks is also evaluated. As shown in Fig. 7B, the Ra values of the Ag-PIII samples do not change obviously after seven cycles of bacteria exposure suggesting that the Ag-PIII samples have stable antibacterial activity. As a surgical prosthesis can be attacked repetitively and rapidly by serum proteins, the effect of serum on the antibacterial activity of Ag-PIII is accessed. As shown in the Fig. 8, no significant difference can be detected from the samples with and without pre-incubation in FBS for 48 h.

3.5. In vivo anti-biofilm property

3.5.1. Radiographical assessment

The radiographic signs of obvious osteolysis, soft tissue swelling, and slight periosteal reaction in all the animals of group I are evaluated by X-ray after 2 weeks. Infection develops as manifested by the persistence of osteolytic lesions and progress of periosteal elevation, new bone formation, and consecutive deformity during the following observation time, but soft tissue swelling disappears after 4 weeks. X-ray taken from group II shows similar but fewer radiographic signs than group I without soft tissue swelling. There is no deformity and soft tissue swelling in group III. Osteolysis and periosteal reaction are less than group II. In group IV, X-rays of two animals does not shown any sign of infection and the rest of the animals show small signs of osteolysis and periosteal reaction compared to the above groups. All the X-ray images acquired from groups V and VI do not show any infection (Fig. 9A).

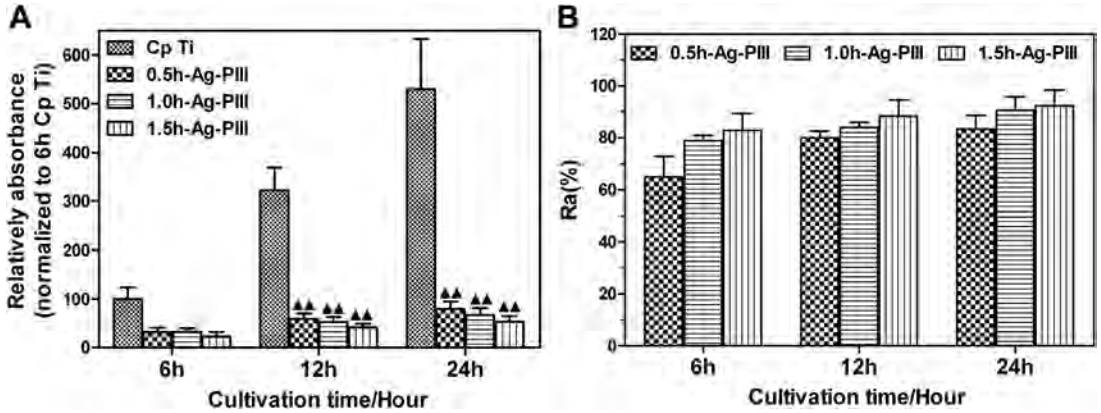

Fig. 3. Biofilm formation on Ag-PIII Ti surfaces. (A) Absorption of crystal violet is used as an indicator of biofilm formation by *S. epidermidis*. The relative absorption of the crystal violet is normalized to that of the 6 h Cp Ti. (B) Antibacterial rates (Ra) are used to estimate the amount of living bacteria on Ag-PIII Ti. ▲▲$p < 0.01$ vs Cp Ti.

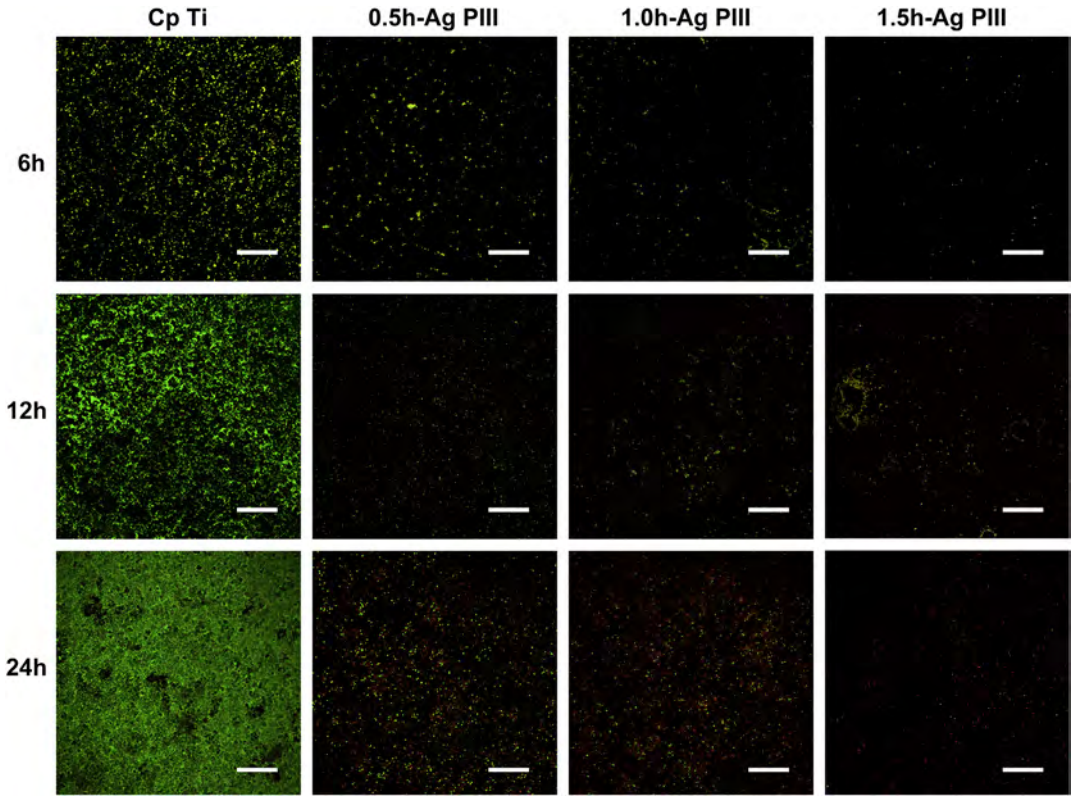

Fig. 4. Projected top views of biofilm formation on the Ag-PIII Ti surface at 6 h, 12 h and 24 h obtained by CLSM after staining with the Baclight dead/live stain. Magnification, ×400. The scale bar is 50 μm.

The average radiographical scores of groups I, II, III, IV, V and VI are 11.8 ± 0.5, 7.2 ± 0.4, 2.8 ± 0.3, 1.9 ± 0.2, 0.3 ± 0.1, and 0.1 after 2 weeks, 12.6 ± 0.3, 11.6 ± 0.3, 5.4 ± 0.1, 2.4 ± 0.1, 0.4 ± 0.1, and 0.1 ± 0.1 after 4 weeks, and 14.5 ± 0.7, 13.3 ± 0.3, 6.9 ± 0.2, 4.4 ± 0.4, 0.5 ± 0.2, and 0.1 ± 0.1 after 6 weeks. There is no significant difference between groups I, II, III, IV and groups V, VI but there are differences among groups I, II, III, and IV. ($p < 0.05$). The trend follows group I > group II > group III > group IV and the radiographical scores increase with observation time. It is consistent with that observed by radiology (Fig. 9B).

3.5.2. Cultures of the implants

Two roll-over cultures of group IV and all cultures of group V remain completely sterile after incubation for 24 h. The bacteria colonies detached from the wires reveal the trend that group I > group II > group III > group IV (Fig. 10A). The findings are

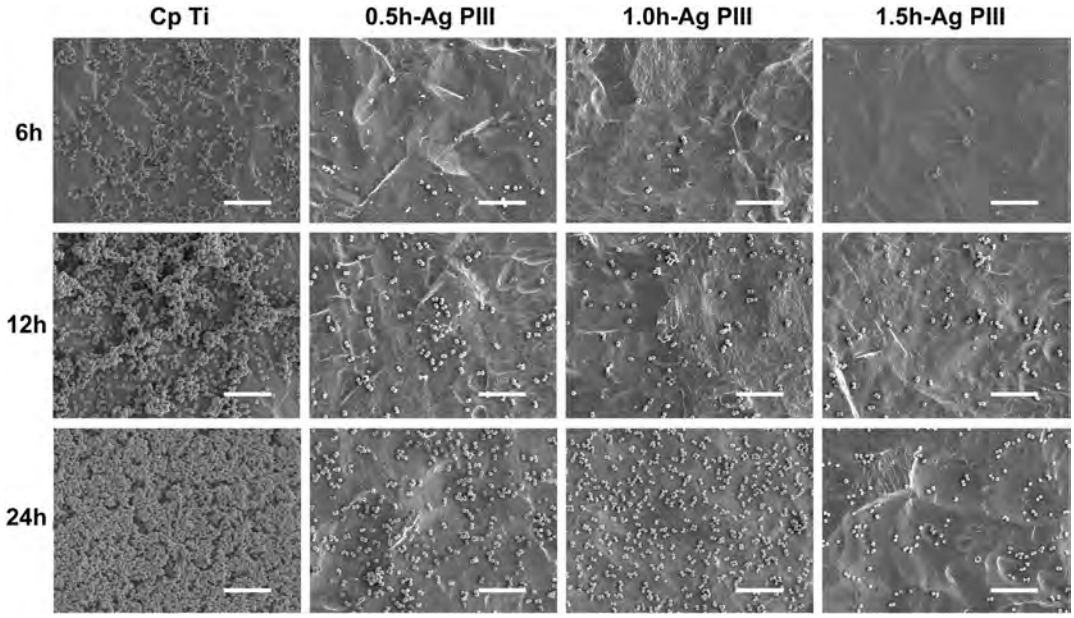

Fig. 5. SEM morphology of biofilm formation on Ag-PIII Ti surface at 6 h, 12 h and 24 h. Magnification, ×2000. The scale bar is 10 μm.

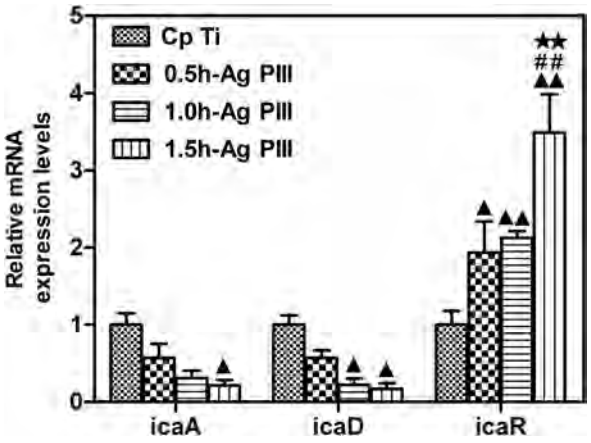

Fig. 6. Relative expressions of *icaAD* and *icaR* by *S. epidermidis* cultured on the Cp Ti and Ag-PIII Ti surface for 24 h, the expression levels of *icaAD* and *icaR* normalized to the 16S rRNA gene. ▲, ▲▲$p < 0.05$, 0.01 vs Cp Ti, # #$p < 0.01$ vs 0.5 h-Ag-PIII Ti, and ★★$p < 0.01$ vs 1.0 h-Ag-PIII Ti.

confirmed by the results of dislodged adhered bacteria after the wires rolling over SBA showing CFU of group I > group II > group III > group IV and no bacteria grow in group V. There are significant differences between group I and groups II, III, and IV, but no significant differences among groups II, III, and IV (Fig. 10B).

3.5.3. Tibia weight and CFU/tibia

The weight of the tibia showing infection by X-ray is obviously greater than the contralateral tibia. As shown in Fig. 11A, the average increased bone weight of group I (226.9 ± 30.1 mg) is significantly larger than that of all the other groups: group II (169.8 ± 45.42 mg), group III (102.9 ± 55.54 mg), group IV (73.2 ± 39.21 mg), group V (14 ± 8.27 mg), and group VI (1.6 ± 5.72 mg). Although no significant differences are found in the increased bone weight between group III and group IV and between group V and group VI, there are significant differences among the other groups.

No bacteria can be cultured from the powder bones in group V and group VI and two bones of group IV also remain sterile. The average amount of CFU per tibia exhibits the trend that group I > group II > group III > group IV. The differences are not statistically significant among groups IV, V, and VI, between group I and group II, and among groups II, III, and IV, but statistically significant among the other groups (Fig. 11B).

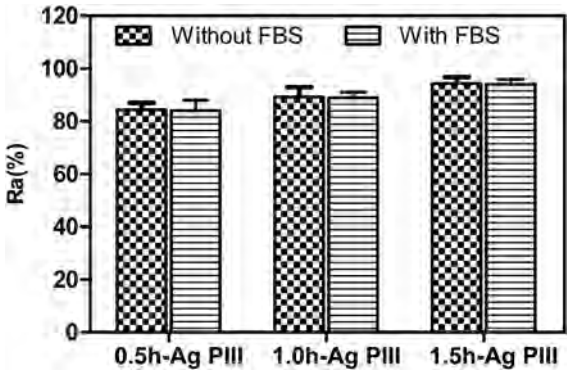

Fig. 8. Antibacterial rates (Ra) of the Ag-PIII Ti pre-incubated with FBS 48 h vs Ra values of the Ag-PIII Ti without pre-incubated with FBS. No differences are found between them.

3.5.4. Histological evaluation

The morphological change on the rat tibia is evaluated by Masson's trichrome staining, while Giemsa staining is employed to identify the bacterial residue. In group I, the histological slices of Masson's trichrome staining show typical signs of bone infection as manifested by development of abscess—lesions, destruction of cortical and cancellous bone, periosteal new bone formation, and the slices of Giemsa staining show that there are lots of bacteria in the intramedullary tissues. In groups II and III, there are relatively minor abscess—lesions, slight bone destruction, and less periosteal new bone formation. The number of bacteria in the intramedullary tissues diminishes obviously. The smallest bone destruction and least amount of bacteria are found from group IV. In groups V and VI, neither detectable signs of infection nor bacteria can be found (Fig. 12A).

The average histological scores of groups I, II, III, IV, V, and VI are 10.8 ± 1.4, 8.4 ± 1.4, 5.3 ± 0.8, 4.7 ± 0.7, 0, and 0, respectively. No significant differences are found between group III and group IV and between group V and group VI, but there are significant differences among the other groups (Fig. 12B).

4. Discussion

Orthopedic surgery may promote the development of implant-associated PPI [33,34], which is a great challenge to the medical community and levies an immense economic burden on society [4,35,36]. Insertion of implants unavoidably disturbs the adjacent

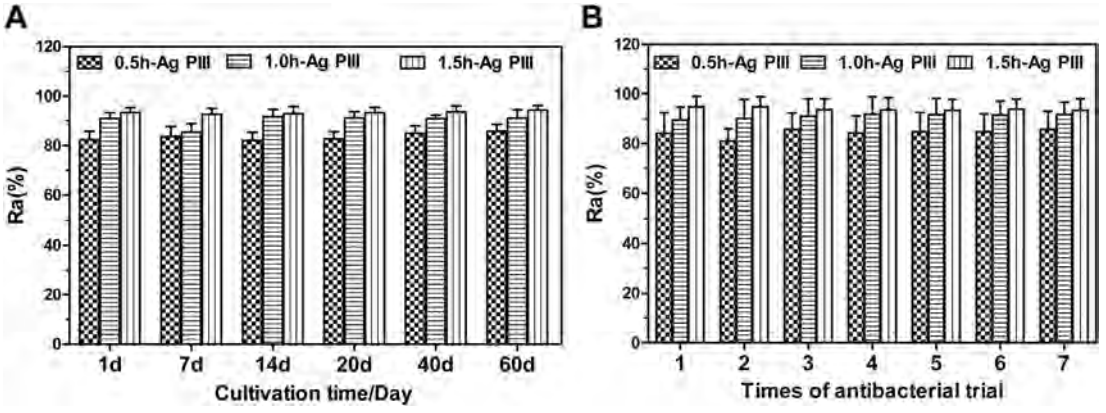

Fig. 7. Antibacterial rates (Ra) of the Ag-PIII Ti after long incubation in an aqueous environment (A) and repeated bacterial attack (B). No significant changes are found from the Ra values of the Ag-PIII Ti after incubation in PBS for up to 60 d and 7 cycles of bacteria exposure.

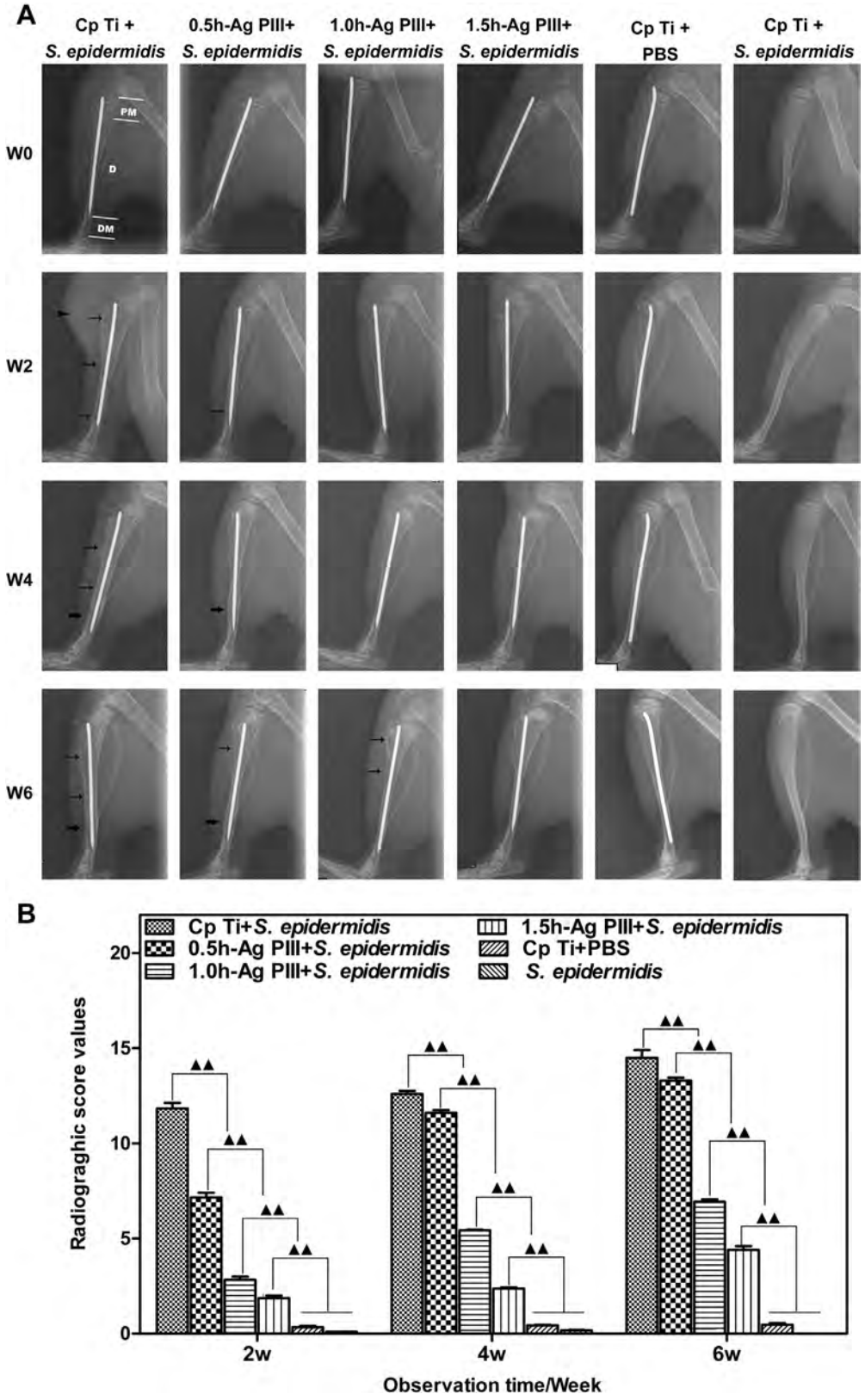

Fig. 9. Radiographical images and evaluation: (A) X-rays of left tibiae in lateral view. Animals in group I: At 2 weeks post-op, clear signs of soft tissue swelling, osteolysis and slight periosteal new bone formation emerge; At 4 weeks post-op, soft tissue swelling disappears, osteolysis is reduced slightly and periosteal new bone formation aggravates; At 6 weeks post-op, osteolysis still exists and periosteal new bone formation reaches its peak. Animals in group II: osteolysis appears at distal diaphysis at 2 weeks post-op; periosteal new bone formation emerges in this place at 4 weeks post-op; at 6 weeks post-op, new osteolysis arises at proximal diaphysis. Animals in group III: only at 6 weeks postop, osteolysis appears at proximal diaphysis. Animals in groups IV, V, and VI: No signs of infection are found. Arrowhead, thin arrow and thick arrow mark soft tissue swelling, osteolysis, and periosteal new bone formation, respectively. White lines mark regions of interest separately assessed for scoring. PM, proximal epi-/metaphysis; D, diaphysis; DM, distal epi-/metaphysis. (B) Radiographical scores of group I–VI. ▲▲$p < 0.01$.

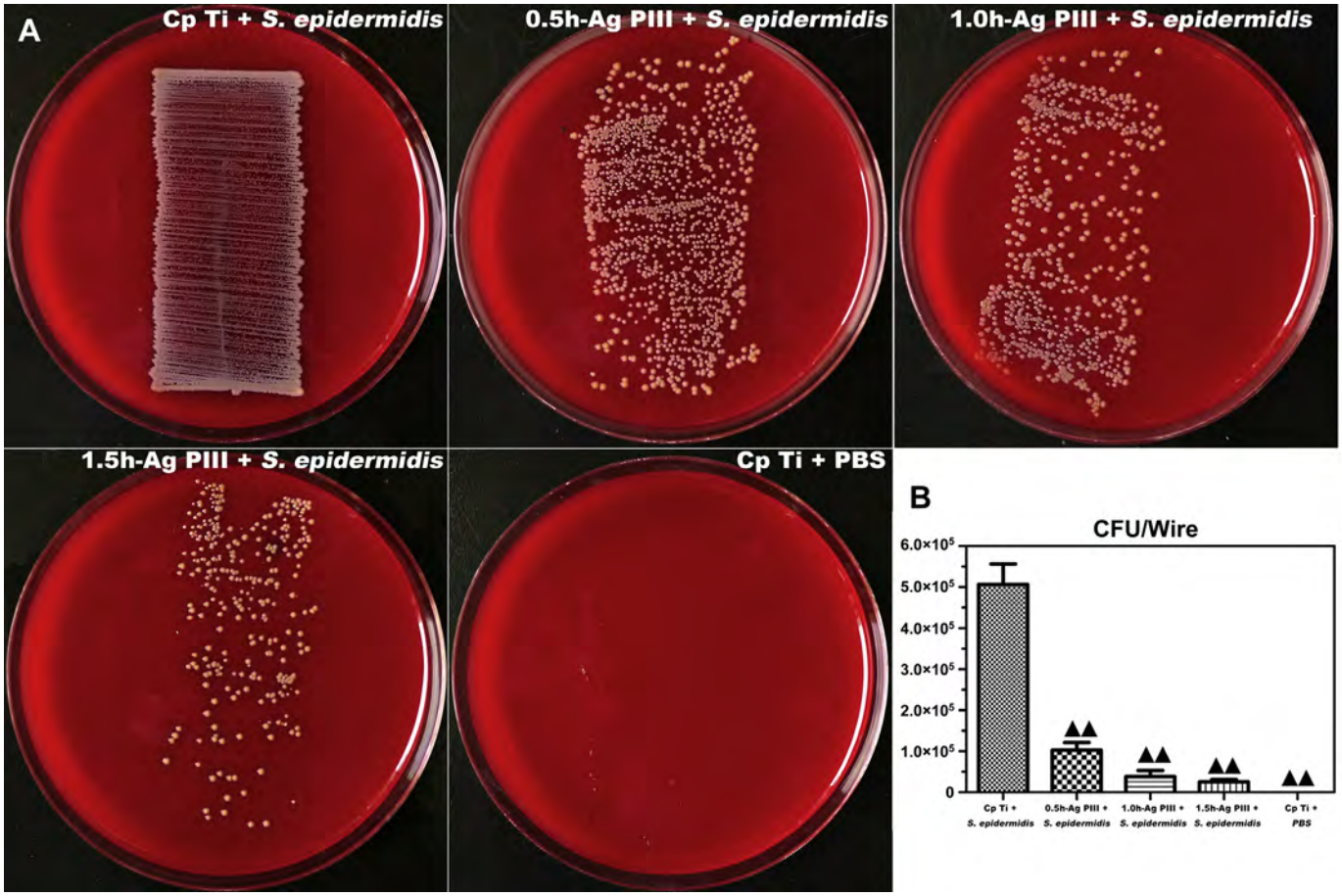

Fig. 10. Cultures of implants: (A) Roll-over cultures obtained from explanted Kirschner wires on day of sacrifice. (B) Counting of the dislodged adhered bacteria after wires rolling over SBA. ▲▲$p < 0.01$ vs group I.

tissues and microcirculation during which bacteria introduced during surgery or hematogenously in the later period may escape the host defense systems growing on the implants transforming into a biofilm which leads to implant-related infection [37,38]. After the development of the biofilm, bacteria become resistant to the immune system and antibiotic therapy [30]. Silver nanoparticles (Ag NPs) having promising antibacterial activity can fight bacterial adhesion and biofilm formation but the small size and high mobility raise safety concerns due to their potential cytotoxicity. In this study, Ag NPs are produced and immobilized *in situ* on titanium by silver plasma immersion ion implantation (Ag-PIII) [21]. By monitoring the *in vitro* and *in vivo* anti-biofilm activity using *S. epidermidis* (ATCC 35984), fabrication and immobilization of Ag NPs on titanium by this technique presents a durable and safe approach to inhibit biofilm formation and minimize PPI.

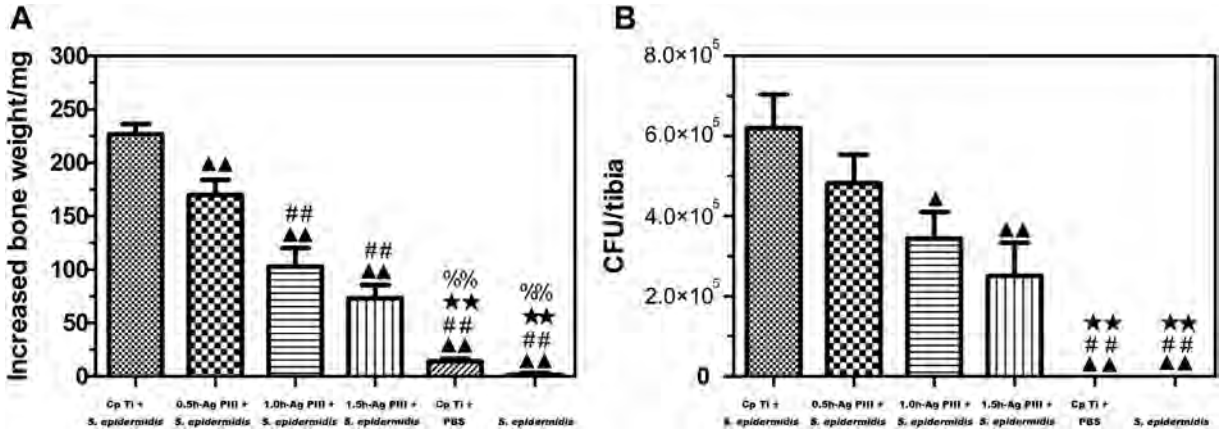

Fig. 11. Indication of bone infection: (A) Increased bone weight of the operated tibia over contralateral tibia. (B) Amount of CFU per tibia, quantified in pulverized bone from operated tibia. ▲, ▲▲$p < 0.05$, 0.01 vs group I, # #$p < 0.01$ vs group II, ★★$p < 0.01$ vs group III, and %% $p < 0.01$ vs group IV.

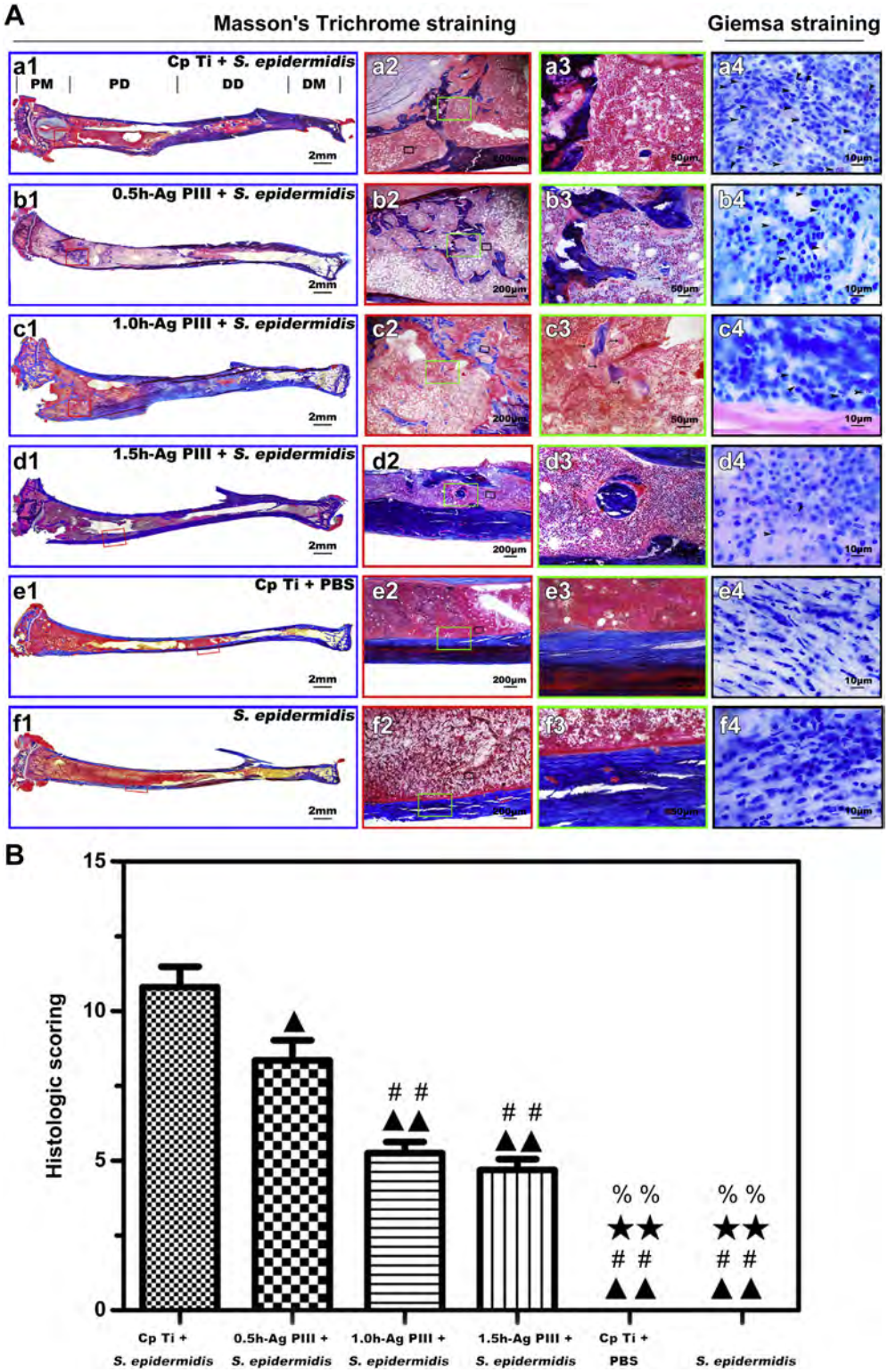

Fig. 12. Histological analysis in rat tibiae at 6 weeks after implantation. (A) Histological slices in a sagittal plane images stained with Masson's Trichrome staining and Giemsa staining. Group I: Overview image (a1) reveals sequestrum formation and destruction of bone. Close-up views (a2–a4) show osteoclasts (arrows) invade bone (a3) and lots of bacteria (arrowheads) persist in the intramedullary tissue (a4). Group II: Overview image (b1) shows enlargement of marrow cavity, destruction and mild remodeling of bone. Close-up views (b2–b4) show osteoclasts invasion of bone (b3) and many bacteria exist in the intramedullary tissue (b4). Group III: Overview image (c1) displays destruction and severe remodeling of cortical bone. Close-up views (c2–c4) show osteoclasts invasion bone (c3) and a small amount of bacteria present in the intramedullary tissue (c4). Group IV: Overview image (d1) shows no obvious bone destruction and remodeling. Close-up views (d2–d4) show no osteoclasts invasion bone and a very small amount of bacteria contamination in the intramedullary tissue (d4). GroupVand VI: No histopathological signs of bone infection are visible. Overview images (e1 and f1) reveal normal bone morphology. Close-up views (e2–e4, f2–f4) show cortical bone intact with no signs of osseous destruction and regular bone marrow without any signs of bacteria. Arrow and arrowhead mark osteoclast and bacteria, respectively. PM, proximal epi-/metaphysis; PD, proximal diaphysis; DD, distal diaphysis; DM, distal epi-/metaphysis. (B) Histological score values of group I–VI. ▲▲$p < 0.01$ vs group I, # #$p < 0.01$ vs group II, ★★$p < 0.01$ vs group III, and %% $p < 0.01$ vs group IV.

The anti-biofilm activity of the Ag-PIII samples is evaluated by a number of distinct techniques and from different perspectives. Crystal violet staining, an agent that is retained in the secreted glycocalyx which is the main ingredient in the biofilm, is used to assess biofilm formation. The other techniques include microbiological counting of the number of viable bacteria, CLSM, and SEM for morphological examination. The results consistently show that Ag-PIII is effective in inhibiting bacteria adhesion. *Staphylococci* biofilm formation is considered to be a two-step process [32,33], bacteria attachment to the foreign surface and formation of a complex biofilm structure which depends mainly on the synthesis of polysaccharide intercellular adhesin (PIA) encoded by the *icaADBC* locus which plays a crucial role in mediating the biofilm formation of *Staphylococcus* [39,40]. A complete PIA synthesis needs the co-expression of *icaA* and *icaD* [28,39] which is adversely regulated by a repressor encoded by the upstream gene *icaR* [41–43]. Real-time PCR results (Fig. 6) indicate that the Ag-PIII samples down-regulate the expression levels of *icaA* and *icaD* but up-regulate the expression levels of *icaR*, indicating that the immobilized Ag NPs not only inhibit bacterial adhesion, but also suppress PIA synthesis. In spite of the encouraging results presented here, further studies need to be done by using other bacteria stains because other species may be involved in implant-associated infection after orthopedic surgery [13,44]. For example, *Pseudomonas aeruginosa* (*P. aeruginosa*), a major human opportunistic pathogen [45], is a commonly isolated organism from the infected orthopedic implant [46], and the biofilm formation mechanism of *P. aeruginosa* is different from that of *S. epidermidis*.

Longevity and safety are crucial to clinical adoption. Bacterial contamination may occur not only peri-operatively but also hematogenously later during the life time of the implant [1]. This problem cannot be circumvented by a releasing strategy because the antibacterial agent will run out eventually, nor by long term administration of prophylactic antibiotics due to the risk of resistance development. According to the results obtained in this work, silver released from the Ag-PIII samples is minimal and the anti-biofilm activity of the Ag-PIII samples does not deteriorate after incubation in PBS for 60 days (Fig. 7A), after multiple cycles of bacteria exposure (Fig. 7B), and even in the presence of serum proteins in the culture medium (Fig. 8). The results indicate that the anti-biofilm action of immobilized Ag NPs is independent of silver release and likely a result of the synergetic effects of silver and the titanium substrate, which is consistent with our previous results [21]. Moreover, according to the results obtained from the CCK-8 assay, the immobilized Ag NPs do not show significant cytotoxicity, whereas concentration dependent toxicity is observed from mobile Ag NPs at a concentration of 8 μg/ml (Fig. 2). The results demonstrate the favorable effects rendered by the immobilized Ag NPs on titanium and the concomitant reduced cytotoxicity.

The anti-biofilm activity of the Ag-PIII samples is assessed *in vivo* using a model of implant-related tibia osteomyelitis in rats, which have been shown to be effective in simulating PPI [25,26]. According to Figs. 9–12, administrating of *S. epidermidis* (10^3 CFU) only is not adequate to induce infection, but infection occurs in the presence of a foreign implant, indicating the implant indeed provides a surface to foster bacterial adhesion and biofilm growth. It is consistent with the clinical observation an implant may promote the onset of infection [47]. In addition, bacterial infection induced bone weight increases are detected from the titanium samples without undergoing Ag-PIII as reflected by periosteal new bone formation, inflammatory cell infiltration, and tissue edema resulting from infection. In comparison, the Ag-PIII samples yield better scores. Microbiological cultures from both the bone powder and implanted Kirschner wires and the histopathological results consistently show that Ag-PIII can reduce the risk of implant-associated PPI. Among the three Ag-PIII samples, the resistance ability to PPI shows the following trend: 1.5 h-Ag-PIII > 1.0 h-Ag-PIII > 0.5 h-Ag-PIII, indicating that the anti-biofilm efficiency is PIII time dependent and consistent with the results obtained *in vitro*.

5. Conclusion

The anti-biofilm characteristics rendered by Ag nanoparticles (NPs) fabricated and immobilized on titanium *in situ* by silver plasma immersion ion implantation is studied using *S. epidermidis* as the bacteria strain. The immobilized Ag NPs do not exhibit apparent cytotoxicity but reduce bacterial biofilm formation *in vitro* by inhibiting bacteria adhesion and *icaAD* transcription. The anti-biofilm activity of the immobilized Ag NPs is independent of silver release, and they can defend several cycles of bacteria exposure *in vitro*, and reduce implant-associated PPI *in vivo*. The effectiveness depends on the Ag-PIII parameters such as time. By using the proper Ag-PIII conditions, Ti can be endowed with anti-biofilm activity, which bodes well for prolonged and safe clinical use by reducing PPI.

Acknowledgments

This work was jointly supported by the National Basic Research Program of China (973 Program, 2012CB933600), the Interdisciplinary (Engineering-Medical) Research Fund of Shanghai Jiao Tong University (Grant No. YG2011MS30), the Opening Project of State Key Laboratory of High Performance Ceramics and Superfine Microstructure (Grant No. SKL201206SIC), the National Natural Science Foundation of China (Grant No. 81271962, 81301571, 31100675), and the Hong Kong Research Grants Council (RGC) General Research Funds (GRF) CityU 112212.

Appendix A. Supplementary data

Supplementary data related to this article can be found online at http://dx.doi.org/10.1016/j.biomaterials.2014.07.040.

References

[1] Hickok NJ, Shapiro IM. Immobilized antibiotics to prevent orthopaedic implant infections. Adv Drug Deliv Rev 2012;64:1165–76.
[2] Stewart PS, Costerton JW. Antibiotic resistance of bacteria in biofilms. Lancet 2001;358:135–8.
[3] Stoodley P, Sauer K, Davies DG, Costerton JW. Biofilms as complex differentiated communities. Annu Rev Microbiol 2002;56:187–209.
[4] Darouiche RO. Treatment of infections associated with surgical implants. N Engl J Med 2004;350:1422–9.
[5] McPherson EJ, Woodson C, Holtom P, Roidis N, Shufelt C, Patzakis M. Periprosthetic total hip infection: outcomes using a staging system. Clin Orthop Relat Res 2002:8–15.
[6] Pulido L, Ghanem E, Joshi A, Purtill JJ, Parvizi J. Periprosthetic joint infection: the incidence, timing, and predisposing factors. Clin Orthop Relat Res 2008;466:1710–5.
[7] Cierny 3rd G, DiPasquale D. Periprosthetic total joint infections: staging, treatment, and outcomes. Clin Orthop Relat Res 2002:23–8.
[8] Fink B, Grossmann A, Fuerst M, Schafer P, Frommelt L. Two-stage cementless revision of infected hip endoprostheses. Clin Orthop Relat Res 2009;467:1848–58.
[9] Toms AD, Davidson D, Masri BA, Duncan CP. The management of periprosthetic infection in total joint arthroplasty. J Bone Joint Surg Br 2006;88:149–55.
[10] Fish DN, Hoffman HM, Danziger LH. Antibiotic-impregnated cement use in U.S. hospitals. Am J Hosp Pharm 1992;49:2469–74.
[11] Huo K, Zhang X, Wang H, Zhao L, Liu X, Chu PK. Osteogenic activity and antibacterial effects on titanium surfaces modified with Zn-incorporated nanotube arrays. Biomaterials 2013;34:3467–78.
[12] Zhao L, Wang H, Huo K, Cui L, Zhang W, Ni H, et al. Antibacterial nanostructured titania coating incorporated with silver nanoparticles. Biomaterials 2011;32:5706–16.

[13] Liu Y, Zheng Z, Zara JN, Hsu C, Soofer DE, Lee KS, et al. The antimicrobial and osteoinductive properties of silver nanoparticle/poly (DL-lactic-co-glycolic acid)-coated stainless steel. Biomaterials 2012;33:8745–56.
[14] Peng ZX, Tu B, Shen Y, Du L, Wang L, Guo SR, et al. Quaternized chitosan inhibits icaA transcription and biofilm formation by *Staphylococcus* on a titanium surface. Antimicrob Agents Chemother 2011;55:860–6.
[15] Zhao L, Chu PK, Zhang Y, Wu Z. Antibacterial coatings on titanium implants. J Biomed Mater Res B Appl Biomater 2009;91:470–80.
[16] Costerton JW. Biofilm theory can guide the treatment of device-related orthopaedic infections. Clin Orthop Relat Res 2005;437:7–11.
[17] Neut D, van de Belt H, Stokroos I, van Horn JR, van der Mei HC, Busscher HJ. Biomaterial-associated infection of gentamicin-loaded PMMA beads in orthopaedic revision surgery. J Antimicrob Chemother 2001;47:885–91.
[18] Loher S, Schneider OD, Maienfisch T, Bokorny S, Stark WJ. Micro-organism-triggered release of silver nanoparticles from biodegradable oxide carriers allows preparation of self-sterilizing polymer surfaces. Small 2008;4:824–32.
[19] AshaRani PV, Low Kah Mun G, Hande MP, Valiyaveettil S. Cytotoxicity and genotoxicity of silver nanoparticles in human cells. ACS Nano 2009;3:279–90.
[20] Pratsinis A, Hervella P, Leroux JC, Pratsinis SE, Sotiriou GA. Toxicity of silver nanoparticles in macrophages. Small 2013;9:2576–84.
[21] Cao H, Liu X, Meng F, Chu PK. Biological actions of silver nanoparticles embedded in titanium controlled by micro-galvanic effects. Biomaterials 2011;32:693–705.
[22] Cao H, Qiao Y, Liu X, Lu T, Cui T, Meng F, et al. Electron storage mediated dark antibacterial action of bound silver nanoparticles: smaller is not always better. Acta Biomater 2013;9:5100–10.
[23] Cao H, Qiao Y, Meng F, Liu X. Spacing dependent antimicrobial efficacy of immobilized silver nanoparticles. J Phys Chem Lett 2014;5:743–8.
[24] Tan H, Peng Z, Li Q, Xu X, Guo S, Tang T. The use of quaternised chitosan-loaded PMMA to inhibit biofilm formation and downregulate the virulence-associated gene expression of antibiotic-resistant staphylococcus. Biomaterials 2012;33:365–77.
[25] Lucke M, Schmidmaier G, Sadoni S, Wildemann B, Schiller R, Haas NP, et al. Gentamicin coating of metallic implants reduces implant-related osteomyelitis in rats. Bone 2003;32:521–31.
[26] Lucke M, Schmidmaier G, Sadoni S, Wildemann B, Schiller R, Stemberger A, et al. A new model of implant-related osteomyelitis in rats. J Biomed Mater Res B Appl Biomater 2003;67:593–602.
[27] Schwab LP, Marlar J, Hasty KA, Smith RA. Macrophage response to high number of titanium particles is cytotoxic and COX-2 mediated and it is not affected by the particle's endotoxin content or the cleaning treatment. J Biomed Mater Res A 2011;99:630–7.
[28] Arciola CR, Campoccia D, Baldassarri L, Donati ME, Pirini V, Gamberini S, et al. Detection of biofilm formation in *Staphylococcus epidermidis* from implant infections. Comparison of a PCR-method that recognizes the presence of ica genes with two classic phenotypic methods. J Biomed Mater Res A 2006;76:425–30.
[29] Christensen GD, Simpson WA, Younger JJ, Baddour LM, Barrett FF, Melton DM, et al. Adherence of coagulase-negative staphylococci to plastic tissue culture plates: a quantitative model for the adherence of staphylococci to medical devices. J Clin Microbiol 1985;22:996–1006.
[30] Antoci Jr V, Adams CS, Parvizi J, Davidson HM, Composto RJ, Freeman TA, et al. The inhibition of *Staphylococcus epidermidis* biofilm formation by vancomycin-modified titanium alloy and implications for the treatment of periprosthetic infection. Biomaterials 2008;29:4684–90.
[31] Chen X, Tsukayama DT, Kidder LS, Bourgeault CA, Schmidt AH, Lew WD. Characterization of a chronic infection in an internally-stabilized segmental defect in the rat femur. J Orthop Res 2005;23:816–23.
[32] Zheng Y, Li J, Liu X, Sun J. Antimicrobial and osteogenic effect of Ag-implanted titanium with a nanostructured surface. Int J Nanomedicine 2012;7:875–84.
[33] Melcher GA, Claudi B, Schlegel U, Perren SM, Printzen G, Munzinger J. Influence of type of medullary nail on the development of local infection. An experimental study of solid and slotted nails in rabbits. J Bone Joint Surg Br 1994;76:955–9.
[34] Petty W, Spanier S, Shuster JJ, Silverthorne C. The influence of skeletal implants on incidence of infection. Experiments in a canine model. J Bone Joint Surg Am 1985;67:1236–44.
[35] NIH Consensus Statement on total knee replacement December 8–10, 2003. J Bone Joint Surg Am 2004;86-A:1328–35.
[36] Gomez J, Rodriguez M, Banos V, Martinez L, Claver MA, Ruiz J, et al. Orthopedic implant infection: prognostic factors and influence of long-term antibiotic treatment on evolution. Prospective study, 1992–1999. Enferm Infecc Microbiol Clin 2003;21:232–6.
[37] Gristina AG, Costerton JW. Bacterial adherence to biomaterials and tissue. The significance of its role in clinical sepsis. J Bone Joint Surg Am 1985;67:264–73.
[38] Gristina AG, Oga M, Webb LX, Hobgood CD. Adherent bacterial colonization in the pathogenesis of osteomyelitis. Science 1985;228:990–3.
[39] Arciola CR, Baldassarri L, Montanaro L. Presence of icaA and icaD genes and slime production in a collection of staphylococcal strains from catheter-associated infections. J Clin Microbiol 2001;39:2151–6.
[40] Rohde H, Frankenberger S, Zahringer U, Mack D. Structure, function and contribution of polysaccharide intercellular adhesin (PIA) to *Staphylococcus epidermidis* biofilm formation and pathogenesis of biomaterial-associated infections. Eur J Cell Biol 2010;89:103–11.
[41] Conlon KM, Humphreys H, O'Gara JP. icaR encodes a transcriptional repressor involved in environmental regulation of ica operon expression and biofilm formation in *Staphylococcus epidermidis*. J Bacteriol 2002;184:4400–8.
[42] Jefferson KK, Pier DB, Goldmann DA, Pier GB. The teicoplanin-associated locus regulator (TcaR) and the intercellular adhesin locus regulator (IcaR) are transcriptional inhibitors of the ica locus in *Staphylococcus aureus*. J Bacteriol 2004;186:2449–56.
[43] Jeng WY, Ko TP, Liu CI, Guo RT, Liu CL, Shr HL, et al. Crystal structure of IcaR, a repressor of the TetR family implicated in biofilm formation in *Staphylococcus epidermidis*. Nucleic Acids Res 2008;36:1567–77.
[44] Moojen DJ, Spijkers SN, Schot CS, Nijhof MW, Vogely HC, Fleer A, et al. Identification of orthopaedic infections using broad-range polymerase chain reaction and reverse line blot hybridization. J Bone Joint Surg Am 2007;89:1298–305.
[45] Balasubramanian D, Schneper L, Kumari H, Mathee K. A dynamic and intricate regulatory network determines *Pseudomonas aeruginosa* virulence. Nucleic Acids Res 2013;41:1–20.
[46] Mousa HA. Infection following orthopaedic implants and bone surgery. East Mediterr Health J 2001;7:738–43.
[47] Andriole VT, Nagel DA, Southwick WO. A paradigm for human chronic osteomyelitis. J Bone Joint Surg Am 1973;55:1511–5.